Removal of Orange G and Rhodamine B dyes from aqueous system using hydrothermally synthesized zinc oxide loaded activated carbon (ZnO-AC)

Jyoti Saini[a], V. K. Garg[b,c*], R. K. Gupta[a], Navish Kataria[c]

[a] *Department of Chemistry, Guru Jambheshwar University of Science and Technology, Hisar 125001, Haryana, India,*

[b]*Centre for Environmental Science and Technology, School of Environment and Earth Sciences, Central University of Punjab, Bathinda - 155001, Punjab, India,*

[c]*Department of Environmental Science and Engineering, Guru Jambheshwar University of Science and Technology, Hisar 125001, Haryana, India*

Graphical Abstract

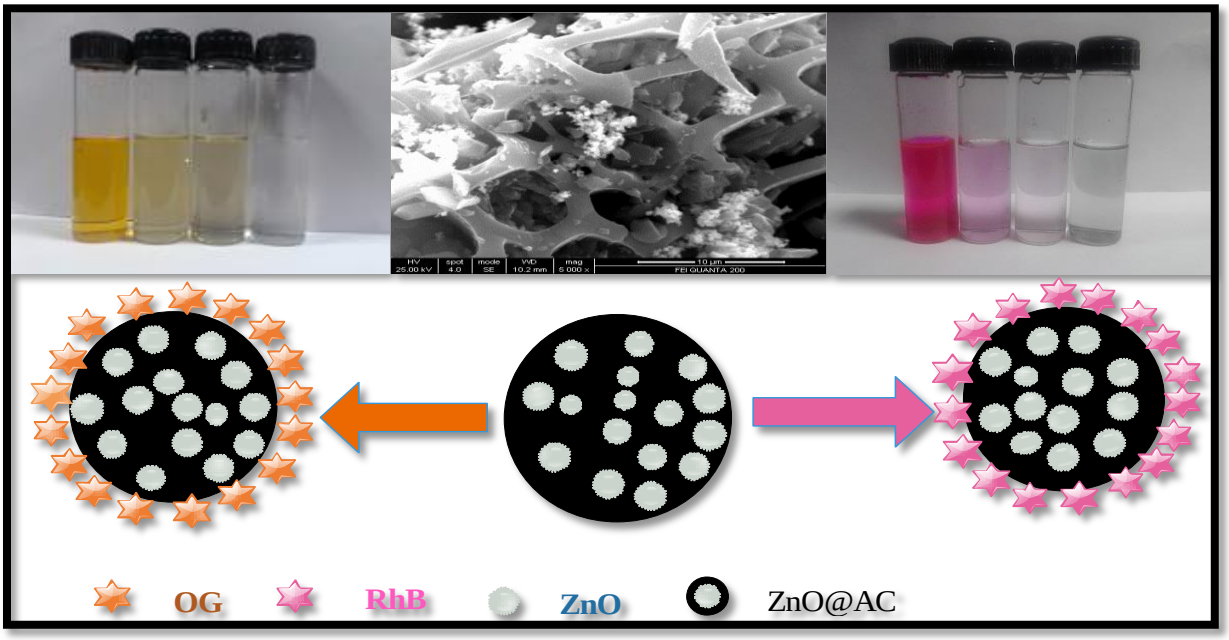

Highlights

- Hydrothermally synthesized ZnO-AC was effective for both acidic and basic dyes.
- Adsorption capacity (q_{max}) for OG and Rh-B was 153.8 and 128.2 mg/g, respectively.
- Langmuir isotherm and pseudo-second order was best fitted in dye adsorption experiments.

Abstract

This study reports the synthesis of zinc oxide loaded activated carbon (ZnO-AC) using hydrothermal method and its use to remove organic dyes [Orange G (OG) and Rhodamine B (Rh-B)] from the aqueous system under varying process conditions. ZnO-AC nanoparticles were characterized using XRD, SEM, EDX, DLS, and FTIR. The Langmuir adsorption model was best fitted in the experimental data for both the dyes. Langmuir adsorption capacity (q_{max}) for OG and Rh-B was 153.8 and 128.2 mg/g, respectively. The rate of adsorption was investigated by various models like pseudo-first-order, pseudo-second-order and intraparticle diffusion model. Rate mechanism was described by pseudo-second-order model for both the dyes. Thermodynamic studies suggested that removal of Rh-B onto ZnO-AC was endothermic up to a temperature of 40 ˚C while OG removal decreased with increase in temperature. Negative values of ΔG^0 for adsorption of dyes suggested spontaneous adsorption processes.

Keywords: Dye removal, ZnO-AC nanoparticle, activated carbon, process parameters, SEM, Kinetics

1 Introduction

Water pollution becomes a major issue for aquatic life, public health and environmental quality. Disposal of dyes laden effluent from various industries including textiles, tanning, paper and pulp is a major environmental concern for industries, municipalities and scientific community. The organic dyes and their degradation products are toxic, carcinogenic and mutagenic for the entire ecosystem. Various chemical and physical methods have been described in the literature for the removal of dyes from the industrial waste water. At this time, adsorption becomes the most familiar technique for wastewater treatment because of its low cost, efficient removal and least sludge generation [1, 2]. In the recent past, nanoparticles are being used in the adsorption of organic dyes and other pollutants due to their specific properties such as large surface area, small particle size, surface charge and thermal stability [3, 4]. Advancement of nanotechnology provides a variety of metal or metal based nanoadsorbents like TiO_2, NiO, SnO_2, MgO, Fe_3O_4, and ZrO_2 for the removal of aqueous pollutants [5-8]. From the literature survey, it was found that, activated carbon is popularly used for removal of textile effluents due to its low cost, large surface area and highly microporous structure [9-12]. Recently, several studies have been reported on removal of basic dyes using adsorbents such as flower shaped ZnO nanoparticle [13], activated carbon media impregnated with zirconium dioxide nanoparticle [9], zinc oxide nanorods loaded on activated carbon [11], etc. Still we needed new, economical and efficient adsorbents. All these studies were focused on either acidic or basic dyes. Keeping these points in mind, this study investigated both acidic and basic dye to compare the adsorption mechanism.

In the present work, zinc oxide deposited activated carbon (ZnO-AC) was synthesized by hydrothermal method and investigated its comparative removal capacity for Orange G (acidic azo dye) and Rhodamine-B (basic dye). ZnO-AC was characterized using different techniques like Fourier transform infrared (FTIR) and Scanning electron microscopy (SEM), X-ray diffraction technique (XRD), Diffraction ray light scattering (DLS). The removal studies were carried out under different conditions, viz., pH,

temperature, contact time, adsorbent dosages and dye concentration for optimization of adsorption conditions. The adsorption capacity of the synthesized nanoparticle was investigated by various adsorption isotherms and kinetic models.

2 Experimental Details

2.1. Materials and Reagents

All the reagents used in this study were of analytical grade. Zinc nitrate hexahydrate, Hexamethylenetetraamine, Activated carbon, and NaOH pallets were obtained from Himedia Laboratory Pvt. Ltd., India. Both the dyes OG and Rh-B were procured from SD fine-Chem Ltd, Mumbai. The physico-chemical properties of dyes are given in Table 1. All the chemicals were used without further purification. The solutions were prepared in deionized water.

2.2. Synthesis and characterization of ZnO-AC

ZnO nanoparticles were synthesized by hydrothermal method [13]. 100 mL of 0.1M solution of Zinc nitrate hexahydrate and 0.1 M Hexamethylenetetraamine was prepared in deionised water and mixed at room temperature. 1.0 M NaOH solution was then added dropwise with continuous stirring into the above mixture, until the pH of the solution raised to 8.0. The mixture thus obtained was refluxed for 6 h at 80˚C. Subsequently white milky suspension was obtained having zinc oxide nanoparticles.

After that, activated charcoal was added to the above suspension (2:1). The suspension was stirred vigorously for 3h. Black precipitates of ZnO-AC nanoparticles were formed, filtered and washed several times with deionized water and ethanol. The obtained precipitate was dried in oven at 70˚C for 2h.

2.3. Instrumentation

The average diameter of synthesized ZnO-AC nanoparticles was determined by dynamic light scattering technique (DLS) (Malvern, UK). The IR spectrum of the sample was obtained on FTIR (Thermo Scientific Nicolet 6700 FT-IR spectrometer, USA). Concentration of dyes was measured by UV-VIS spectrophotometer (LABINDIA, Model UV-VIS 3000^{+}). The λ_{max} of OG (475 nm) and Rh-B (554 nm) was determined by UV-

VIS. The X-ray pattern of ZnO-AC was recorded on XRD (PANalytical X'Pert Pro Multipurpose Diffractometer (MPD) (PW3040/60 X-ray generator, Netherlands), having Cu-K_α X-ray (λ=1.5418 Å) generating 40 kV accelerating voltage and 40 mA emission current. The surface images and elemental characteristics of sample were obtained by Scanning electron microscope (SEM) and Energy-dispersive X-ray spectroscopy (EDX) using ICON-Quanta 200 Mark II Environmental scanning Electron Microscope.

2.4. Adsorption experiments

All the batch mode experiments were done by shaking 0.02 g ZnO-AC and 50 mL of 50mg/L OG and Rh-B at pH 7 for 140 minutes except for pH variation experiments. All experiments were done in dark conditions to avoid photocatalysis. These experiments were performed at different process conditions like pH, temperature, time, adsorbent dose and adsorbate concentration to obtain rates and equilibrium conditions. The absorbance and hence the concentration of both the dyes before and after the treating with ZnO-AC were measured by spectrophotometer.

The adsorption capacity (q_e, mg/g) and dye removal percentage (%) were calculated using below given equations:

$$Adsorption\ capacity\ (q_e) = \frac{(C_o - C_e)\,V}{m} \quad (1)$$

$$Dye\ removal\ (\%) = \frac{(C_o - C_e)}{C_o} \times 100 \quad (2)$$

where C_0 (mg/L) and C_e (mg/L) are respectively the initial and equilibrium concentration of dye stuff, q_e (mg/g) denotes adsorption capacity, V is the volume of solution (L) and m is the mass of adsorbent (g) in the above equations.

3 Results and Discussion

3.1 Characterization of adsorbents

ZnO-AC nanoparticles were characterized by XRD, SEM, DLS, FTIR, and EDX as described below:

3.1.1. XRD analysis

XRD pattern of synthesized nanoparticles was detected by diffraction angle 2θ and peak intensity. The designated peaks at 2θ 32.13˚, 34.73˚, 36.62˚, 47.7˚, 56.95˚, 63.17˚, 66.79˚, 68.21˚and 69.39˚ revealed the hexagonal structure of prepared nanoparticles and denoted diffraction plane or miller indices (hkl) (100), (002), (101), (102), (110), (103), (200), (112) and (201) respectively (Fig 1). The XRD pattern of synthesized ZnO nanoparticles reassembled to the standard ZnO. The lattice parameter for synthesized nanoparticle was calculated by the following d-interplanar spacing equation [9];

$$\frac{1}{d_{hkl}^2} = \frac{4}{3}\left(\frac{h^2 + hk + k^2}{a^2}\right) + \frac{l^2}{c^2} \qquad (3)$$

The calculated mean value of a = 3.240 and c = 5.20 from the above equation illustrates the hexagonal structure of ZnO. Further, broadband at 2θ 26.2˚ and 44.7˚ for activated carbon may be due to amorphous properties of the material. The peak intensity of ZnO-AC was slightly lower than pristine ZnO which indicate the agglomeration of ZnO nanoparticles on the surface of AC.

3.1.2. FTIR analysis

The presence of different functional groups in the synthesized ZnO-AC was characterized by FTIR (Fig. 2). A sharp peak at 475 cm^{-1} was observed due to ZnO stretching. The wide peak detected at ~950 cm^{-1} was due to C-H bending vibrations. The Peaks occurred at 1210-1320 cm^{-1} may be due to C-OH stretching vibrations. The peak spotted at 1702 cm^{-1} attributed to C=O stretching vibration. Spiky peaks observed at 2332 cm^{-1} and 2362 cm^{-1} may be attributed to symmetric and asymmetric stretching

vibrations of CH_2 bonds. A broad absorption at 3300-3400 cm^{-1} was assigned to O-H stretching vibrations. [11]. Increase in peak intensities was observed in ZnO-AC as compared to pristine AC.

3.1.3. Surface Morphology

The SEM images of ZnO-AC nanoparticles are given in Fig. 3(a-d). The SEM images displayed agglomerated zinc oxide nanoparticles on the activated carbon surface. ZnO-AC nanoparticles are distributed randomly over the AC surface. Photographic images of exhausted material are given in Fig. 4(a-d). The weight percent of the detected elements were Zn 10.02, C 81.85, O 8.15, and atomic percent was 91.15, 6.80, and 2.05. There were no additional energy peaks observed in the EDX spectrum (Fig 5). The observed hydrodynamic diameter of ZnO-AC ranged between 200-1000 nm as shown in Fig. 6. However the hydrodynamic diameter of agglomerated ZnO nanoparticles was found to be below 200 nm. These ZnO nanoparticles were observed in agglomerate form on the surface of activated carbon. .

3.2 Adsorption Experiment

3.2.1. Effect of pH

The effect of pH of the solution on the adsorption of Rh-B and OG is presented in Fig. 7a. Experiments were performed with pH (2.0-10) for 50mL of 50 mg/L dyestuff and the adsorbent dose of 0.02 g. Rh-B adsorption increases from 92% to 96% with an increase in pH (2.0-7.0), further there is no significant change at higher pH. At lower pH, absorbent surface generates net positive charge due to higher concentration of H^+ ions. As a result, there is an electrostatic repulsion between Rh-B molecules and adsorbent surface which inhibits the Rh-B removal [14]. On the contrary, the maximum removal of the OG is 99.6% at pH 2 and slightly decreased from 99.6% to 95.8% with increasing pH upto10. Higher OH^- ions generate a net negative charge on the adsorbent surface which

competes with OG ions. These results revealed that cationic and anionic dyes require basic and acidic, medium for maximum removal [15].

3.2.2. Effect of contact time

Fig. 7b shows the removal percentage of OG and Rh-B. All the experiments were carried out at pH 7, 50 mL of 50 mg/l OG and Rh-B and 0.02 g of adsorbent dose for different ranges of time (5-120 min.). Rh-B removal was increased from 54.8% to 94.6% with a contact time (5-120 min.), and for OG it was 58.5% to 99.2%. The adsorption of both the dyes was rapid. The experiment revealed that adsorption equilibrium reached in 100 min. and after that lesser change was observed in adsorption of both the dyes. This may be attributed to low availability of active sites onto the adsorbing surface.

3.2.3. Effect of dose

The effect of adsorbent dose for the adsorption of Rh-B and OG was reported in Fig 8a, b. These experiments were studied over the range (0.008-0.03g) adsorbent dosages, 50 mL of 50 mg/l of OG and Rh-B at pH 7. The results indicated that the percent removal of both the dyes increased up to 99.2 % by raising the adsorbent dose from (0.008-0.03g). This may be due to the increase in surface area and adsorption sites with increase in adsorbent dose. These observations are similar to observations reported by other studies [14, 16] for the adsorption of Rh-B and OG by treated biomass and mesoporous carbon material.

3.2.4. Effect of temperature

The experiment was performed at (283-343 K) temperature, and other process parameters were kept constant. The results are given in Fig. 9. The adsorptive removal of Rhodamine B increased from 92.0% to 99.5% with increasing temperature, which suggested the endothermic nature of the process. It may be attributed to increase diffusion of adsorbate molecules towards the external boundary layer. Elevated temperature also enhances the intraparticle diffusion of adsorbate ions into the pores [17]. In contrast, OG

removal was decreased from 99.2% to 94.1% with an increase in temperature. This trend indicated exothermic characteristics of the process. It may be explained as adsorbate molecules moved from a solid phase to bulk phase causing desorption phenomenon at high temperature [18].

3.3 Adsorption kinetics

Pseudo-first-order and Pseudo-second-order models were applied to the data to compare the adsorption mechanism for both the dyes.

Pseudo first order equation expressed as [19];

$$\log(q_e - q_t) = \log q_e - \left(\frac{k_1}{2.303}\right) t \qquad (4)$$

where q_e (mg/g) is the amount of adsorbate adsorbed at equilibrium and q_t (mg/g) is the amount of adsorbate adsorbed at time t, k_1 (min^{-1}) is the pseudo-first-order rate constant and t is the time (min^{-1}). A Plot of log ($q_e - q_t$) versus t used to determine the pseudo-first-order rate constant k_1 and adsorption capacity q_e for OG and Rh-B (Fig. 10a). The calculated correlation coefficient R^2 for OG and Rh-B was 0.8548 and 0.8756 respectively (Table 2). Value of correlation coefficient was small for both the dyes and there were large difference between experimental adsorption capacity and calculated from the model. Hence, these results suggested that pseudo-first order model is not applicable to describe the adsorption kinetics of both the dyes.

Pseudo second order model is represented by [20]:

$$\frac{t}{q_t} = \frac{1}{k_2\, q_e^2} + \frac{t}{q_e} \qquad (5)$$

Here k_2 is the pseudo-second order rate constant. A plot between $\frac{t}{q_t}$ versus t was applied to determine the second order rate constant k_2 and adsorption capacity (q_e) . Correlation coefficient ($R^2 \geq 0.999$) is very high for both the dyes (Fig. 10b). The calculated (q_e) values were almost similar to experimental (q_e) values (Table 2).

Therefore, the pseudo-second order model reported good consistency with the adsorption kinetics of both dyes.

The intraparticle diffusion model is expressed as [21];

$$q_t = k_{id}\, t^{1/2} + C \tag{6}$$

k_{id} is the intraparticle diffusion rate constant. Intercept value C indicates the thickness of the boundary layer. The value of k_{id} and C were calculated from the plot between $t^{1/2}$versus q_t shown in Fig. 10c. If the plot between $t^{1/2}$and q_t is pass through the origin, then intraparticle diffusion is the rate determining step. Hence the line did not pass through origin; this phenomenon does not apply in the present case. Here possibility of both intraparticle diffusion and boundary layer effect influence on rate controlling step. The calculated correlation coefficient for both dyes was ($R^2 \geq 0.9407$). These results indicate that adsorption of the OG and Rh-B is a complex process consisting of intraparticle diffusion and boundary layer effect [22].

3.4. Adsorption isotherm

The adsorption capacity and interaction between adsorbent and adsorbate were described by adsorption isotherms. Langmuir and Freundlich adsorption isotherms were used to optimize the design of adsorption system. A linear form of the Langmuir model may be written as [23];

$$\frac{C_e}{q_e} = \frac{1}{q_{max} b} + \frac{C_e}{q_{max}} \tag{7}$$

where, Q_{max} (mg/g) is the monolayer adsorption capacity, and b (L/mg) is the Langmuir constant related to the affinity of binding sites. A linear plot was obtained between C_e/q_e versus C_e for both the dyes as shown in Fig. 11ab. The monolayer

adsorption capacities for OG and Rh-B were found to be 153.84 mg/L and 128.20 mg/L respectively (Table 3). The correlation coefficient values were ($R^2 \geq 0.997$) for both the dyes. The adsorption capacity of ZnO-AC has been compared with available literature. It has been found that adsorption capacity of ZnO-AC for both dyes is more than several other adsorbents studied in yesteryears (Table 4).

Freundlich isotherm model assumes the multilayer adsorption phenomenon. Freundlich model in linear form is represented by the following equation [24];

$$logq_e = logK_f + \frac{1}{n}\, logC_e \qquad (8)$$

where K_f (mg/g(L/mg)$^{1/n}$) is Freundlich constant related to adsorption capacity and $1/n$ indicates intensity of adsorption. The value of K_f and n were obtained from the linear plot between log q_e versus log C_e (Fig. 11cd). The value of n is complementary to the adsorption process. The value of n should lie in the ranges 1-10 for favorable adsorption conditions. The calculated correlation coefficients for OG (R^2 =0.858) and Rh-B (R^2 =0.735) were low (Table 3). These results demonstrated that Freundlich model was not fitted to the experimental data.

Langmuir isotherm provides high correlation coefficient values, consequently best fitted to the experimental data for both the dyes.

3.5. Thermodynamic study

Thermodynamic studies were done to elaborate the thermodynamic parameters. Experiments were carried out in the temperature ranges (10 - 70 ˚C) keeping all the parameters constant. Enthalpy (ΔH^o), entropy (ΔS^o) and change in Gibb's free energy (ΔG^o) were calculated for both the dyes by using Van't Hoff equation [25]:

$$\Delta G^0 = -RTlnK_d \qquad (9)$$

$$K_d = \frac{C_m}{C_e} \quad (10)$$

$$\Delta G^0 = \Delta H^0 - T\Delta S^0 \quad (11)$$

where K_d is the equilibrium constant expressed by following equation, C_m (mg/L) is the amount of dye on adsorbent. A plot between ln K_d versus 1/T was used to calculate the value of (ΔH^o) and (ΔS^o) [Table 5]. The negative value of ΔG^0 indicates the feasibility and spontaneousness of the adsorption of both the dyes onto ZnO-AC. The adsorption of Rh-B increases with increasing temperature. The positive value of ΔH^0(28.04 k J mol^{-1}) designated endothermic nature of the adsorption process [26]. However, the results of OG were reverse to Rh-B, the amount of adsorbed dye decreased with increase in temperature. The negative values of ΔH^o (-33.31 k J mol^{-1}) indicates an exothermic adsorption phenomenon [18].

4 Conclusion.

ZnO-AC nanoparticles have been synthesized via hydrothermal method and used for removal of Rhodamine-B and Orange G. The advantage of the present work is the maximum adsorption capacity of Rh-B (128.2 mg/g) and OG (153.8 mg/g) by using 0.02g adsorbent dose. Langmuir isotherm model best fits in the experimental data than the Freundlich model. Adsorption capacity increases with increasing temperature for Rh-B while it decreases for OG. The pseudo-second-order kinetic model best describes the adsorption kinetics of Rh-B and OG onto ZnO-AC. The present study interpreted that ZnO-AC nanoparticles act as effective adsorbent for both acidic as well as basic dyes.

References

1. V. K. Garg, R. Gupta, A. Yadav, R. Kumar, Dye removal from aqueous solution by adsorption on treated sawdust, Bioresource Technology. 89 (**2003**) 121–124.
2. L. Zheng, C. Wang, Y. Shu, X. Yan, L. Li, Utilization of diatomite/chitosan–Fe (III) composite for the removal of anionic azo dyes from wastewater: Equilibrium, kinetics and thermodynamics, Colloids and Surfaces A. 468 (**2015**) 129–139.

3. R. Chen, W. Wang, X. Zhao, Y. Zhang, S. Wu, F. Li, Rapid hydrothermal synthesis of magnetic CoxNi1_xFe_2O_4 nanoparticles and their application on removal of Congo red, Chemical Engineering Journal. 242 (**2014**) 226–233.
4. U. K. Gautam, L. S. Panchakarla, B. Dierre, X. Fang, Y. Bando, T. Sekiguchi, A. Govindaraj, D. Golberg, C. N. R. Rao, Solvothermal Synthesis, Cathodoluminescence, and Field-Emission Properties of Pure and N-Doped ZnO Nanobullets, Advance Functional Materials. 19 (**2009**) 131–141.
5. S. Hashemian, A. Foroghimoqhadam, Effect of copper doping on $CoTiO_3$ limenite type nanoparticles, Chemical Engineering Journal. 235 (**2014)** 299–306.
6. I. Khosravi, M. Eftekhar, Evaluation catalytic efficiency of $NiFe_2O_4$ nano spinel in removal of reactive dye from aqueous solution, Powder Technology. 250 (**2013**) 147–153.
7. Y. Haldorai, J. Shim, An efficient removal of methyl orange dye from aqueous solution by adsorption onto chitosan/MgO composite: A novel reusable adsorbent, Applied Surface Science. 292 (**2014)** 447– 453.
8. R. Sandoval, A. Cooper, K. Aymar, A. Jain, K. Hristovski, Removal of arsenic and methylene blue from water by granular activated carbon media impregnated with zirconium dioxide nanoparticles, Journal of Hazardous Materials. 193 (**2011**) 296–303.
9. M. Ghaedi, M. Ghayedi, S. Kokhdan, R. Sahraei, Palladium, silver, and zinc oxide nanoparticles loaded on activated carbon as adsorbent for removal of bromophenol red from aqueous solution, Journal of Industrial and Engineering Chemistry. 19 (**2013**) 1209–1217.
10. M. Ghaedi, F. Karimi, B. Barazesh, R. Sahraei, A. Daneshfar, Removal of Reactive Orange 12 from aqueous solutions by adsorption on tinsulfide nanoparticle loaded on activated carbon, Journal of Industrial and Engineering Chemistry. 19 (**2013**) 756–763.

11. M. Ghaedi, A. Nasab, S. Khodadoust, R. Sahraei, A. Daneshfar, Characterization of zinc oxide nanorods loaded on activated carbon as Cheap and efficient adsorbent for removal of methylene blue, Journal of Industrial and Engineering Chemistry. 21 (**2015**) 986–993.
12. F. Ansari, M. Ghaedi, M. Taghdiri, A. Asfaram , Application of ZnO nanorods loaded on activated carbon for ultrasonic assisted dyes removal: Experimental design and derivative spectrophotometry method, Ultrasonics Sonochemistry. 33 (**2016**) 197-209
13. N. Kataria, V. K. Garg, M. Jain, K. Kadirvelu, Preparation, characterization and potential use of flower shaped Zinc oxide nanoparticles (ZON) for the adsorption of Victoria Blue B dye from aqueous solution, Advanced Powder Technology**. 2**7 **(2016)** 1180–1188.
14. H. Lata, V.K. Garg, R. K. Gupta, Adsorptive removal of basic dye by chemically activated Parthenium biomass: equilibrium and kinetic modeling, Desalination. 219 (**2008**) 250–261

15. I. Mall, V. Srivastava, N. Agarwal, Removal of Orange-G and Methyl Violet dyes by adsorption onto bagasse fly ash and kinetic study and equilibrium isotherm analyses, Dyes and Pigments. 69 (**2006)** 210-223.
16. K Arzani, B G. Ashtiani, A. H. A. Kashi, Equilibrium and Kinetic Adsorption Study of the Removal of Orange-G Dye Using Carbon Mesoporous Material, Journal of Inorganic Materials. 27 **(2012)**
17 L. Peng, P. Qin, M. Lei, Q. Zeng, H. Song, Y. Jiao, J. Shao, B. Liao, J. Gu, Journal of Hazardous Materials. 209-210 (**2012**) 193–198.
18 L. Doumic, G. Saliernob, M. Cassanello, P. Haure, M. Ayude, Efficient removal of Orange G using Prussian Blue nanoparticles supported over alumina, catalysis Today. 240 (**2015)** 67–72.

19 S. Lagergren, About the theory of so-called absorption of soluble substances, Kungliga Svenska Vetenskapsakademiens Handlingar. 24 (**1898**) 1–3.

20 Y. S. Ho, G. McKay, Pseudo-second order model for sorption processes, Biochemistry. 34 (**1999**) 451–465.

21 W. Weber, J. Morris, Kinetics of adsorption on carbon from solution, Journal of the sanitary engineering division. 89 (**1963**) 31–60.

22 C. Duran, D. Ozdes, A. Gundogdu, H. Senturk, Kinetic and isothermanalysis of basic dyes adsorption onto almond shell as a low cost adsorbent, Journal of Chemical Engneering Data. 56 (**2011**) 2136–2147.

23 I. Langmuir, The adsorption of gases on plane surfaces of glass, mica and platinum, Journal of the American Chemical society. 40 (**1918)**, 1361–1403.

24 H. Freundlich, Uber die adsorption in lasugen, Journal of Physical Chemistry. 57 (**1906**) 385–470.

25 J. M. Smith, Ness HCV, Introduction to Chemical Engineering Thermodynamics. McGraw-Hill New York, USA, **1987**.

26 K. Liu, H. Li, Y. Wang, X. Gou, Y. Duan, Adsorption and removal of rhodamine B from aqueous solution by tannic acid functionalized graphene, Colloids and Surfaces A. 477 (**2015)** 35–41.

27 K. Kadirvelu, C. Karthika, N. Vennilamani, S. Pattabhi, Activated carbon from industrial solid waste as an adsorbent for the removal of Rhodamine-B from aqueous solution: Kinetic and equilibrium studies, Chemosphere. 60 (**2005**) 1009–1017

28 S. Khamparia, D. Jaspal Investigation of adsorption of Rhodamine B onto a natural adsorbent Argemone mexicana Journal of Environmental Management.183 (**2016**) 786-793

29 L. Peng, P. Qina, M. Lei, Q. Zenga, H. Songa, J. Yanga, J. Shaoa, B. Liaoa, J. Gua, Modifying Fe_3O_4 nanoparticles with humic acid for removal of Rhodamine B in water, Journal of Hazardous Materials. 209– 210 (**2012**) 193– 198

30 F. N. Azad, M. Ghaedi, K. Dashtian, S. Hajati, A. Goudarzic , M. Jamshidia, Enhanced simultaneous removal of malachite green and safranin O by ZnO nanorod-loaded activated carbon: modeling, optimization and adsorption isotherms, New Journal of Chemistry.,39 (**2015**) 7998—8005

31 L. Hu, H. Yuan, L. Zou, F. Chen, X. Hu, Adsorption and visible- light driven photocatalytic degradation of Rhodamine B in aqueous solutions by Ag@AgBr/SBA-15, Applied Surface Science. 335 (**2015**) 706-715

32 D. Wan, G. Wang, W. L. K. Chen, L. L. Q. Hu, Adsorption and heterogeneous degradation of rhodamine B on the surface of magnetic bentonite material, Applied Surface Science. 349 (**2015**) 988-996

33 S. Hajati, M Ghaedi, F Karimi, B. Barazesh, R. Sahraei, A. Daneshfar, Competitive adsorption of Direct Yellow 12 and Reactive Orange 12 on ZnS:Mn nanoparticles loaded on activated carbon as novel adsorbent, Journal of Industrial and Engineering Chemistry. 20(**2014**) 564–571

34 G. S. Dawood, Removal Orange (G) Dye from aqueous solution by adsorption on Bentonite, Tikrit Journal of Pure Science. 15 (**2010**) 231-235.

Caption of figure

Figure 1 XRD patterns of AC, ZnO and ZnO-AC nanoparticles.

Figure 2 FT-IR spectrum of AC and ZnO-AC nanoparticles.

Figure 3 (a-d) SEM image of ZnO-AC nanoparticles.

Figure 4 (a, b) SEM images of ZnO-AC nanoparticles after OG adsorption (c, d) SEM images of ZnO-AC nanoparticles after Rh- B adsorption.Figure 5 EDX of ZnO-AC nanoparticles.

Figure 6 DLS of ZnO-AC nanoparticles

Figure 7 (a) Effect of pH on adsorption of Rh-B and OG dye on ZnO-AC nanoparticles (a) (b) Effect of contact time adsorption of Rh-B and OG dye on ZnO-AC nanoparticles.

Figure 8 Adsorption of Rh-B and OG dye on ZnO-AC nanoparticles (a) effect of dye concentration with adsorbent dose for Rh-B (b) effect of dye concentration with adsorbent dose for OG.

Figure 9 Effect of temperature for adsorption of Rh-B and OG dye on ZnO-AC nanoparticles.

Figure 10 Kinetic plots for adsorption Rh-B and OG dye on ZnO-AC nanoparticles (a) pseudo-first order plot (b) pseudo-second order plot (c) intraparticle diffusion plot.

Figure 1110 Adsorption isotherms plots for OG and Rh-B dye on ZnO-AC nanoparticles (a, b) Langmuir isotherm plot (c, d) Freundlich isotherm plot for OG and Rh-B dye respectively.

.

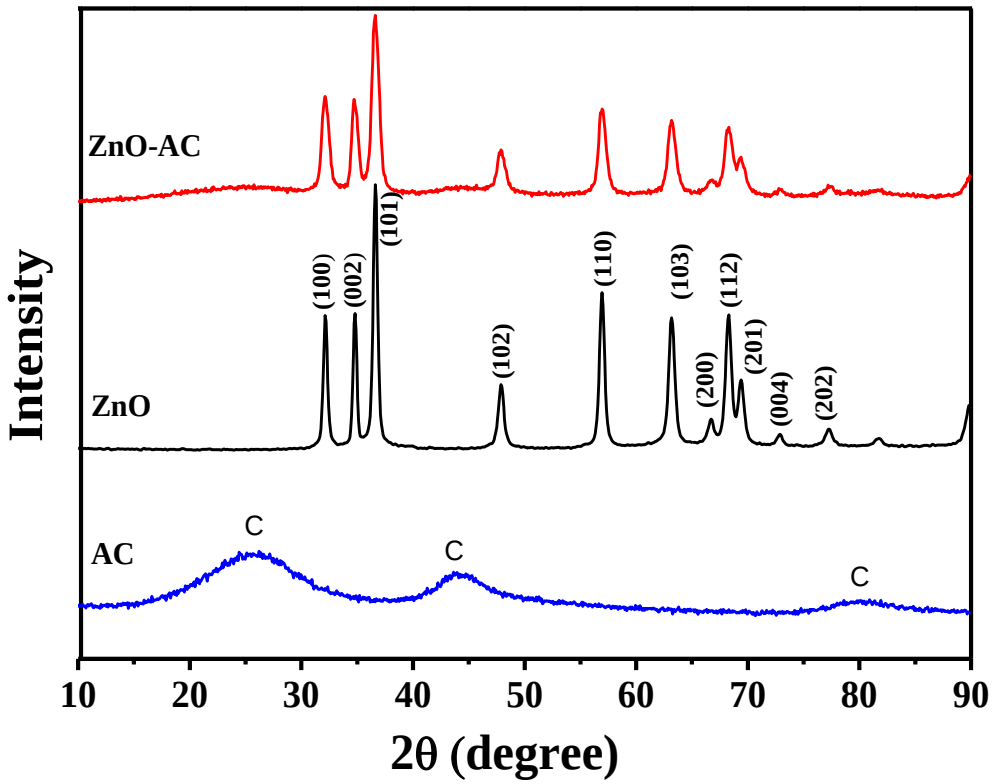

Figure 1 XRD patterns of AC, ZnO and ZnO-AC nanoparticles

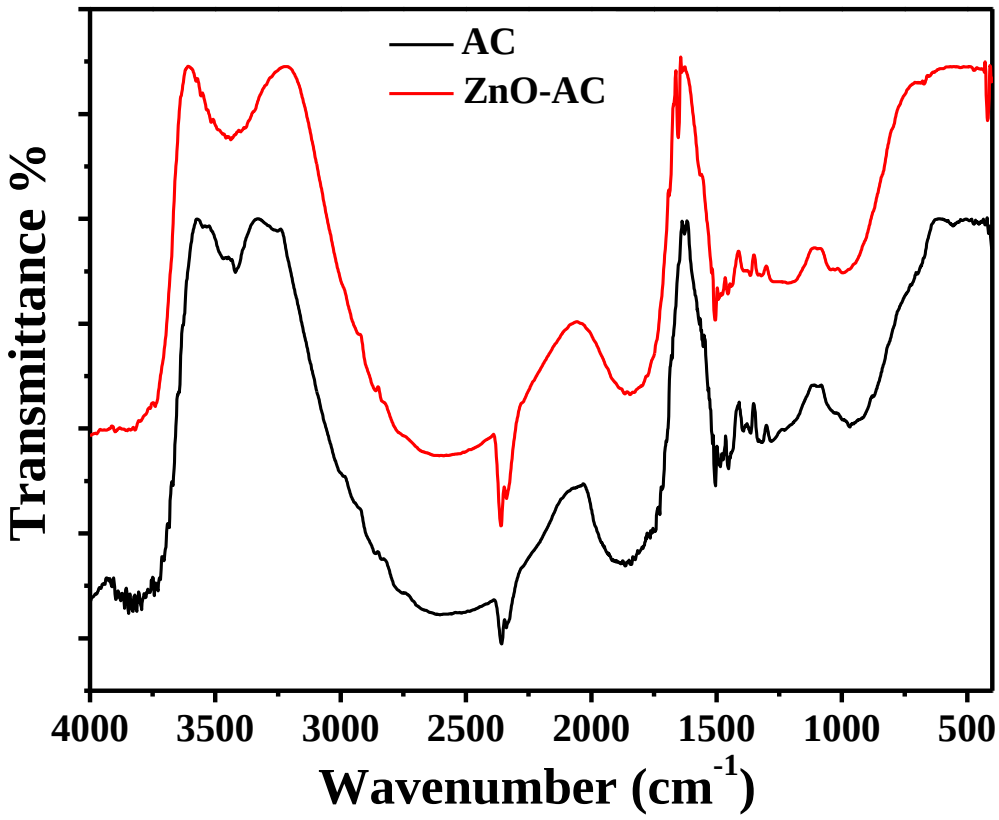

Figure 2 FT-IR spectrum of AC and ZnO-AC nanoparticles

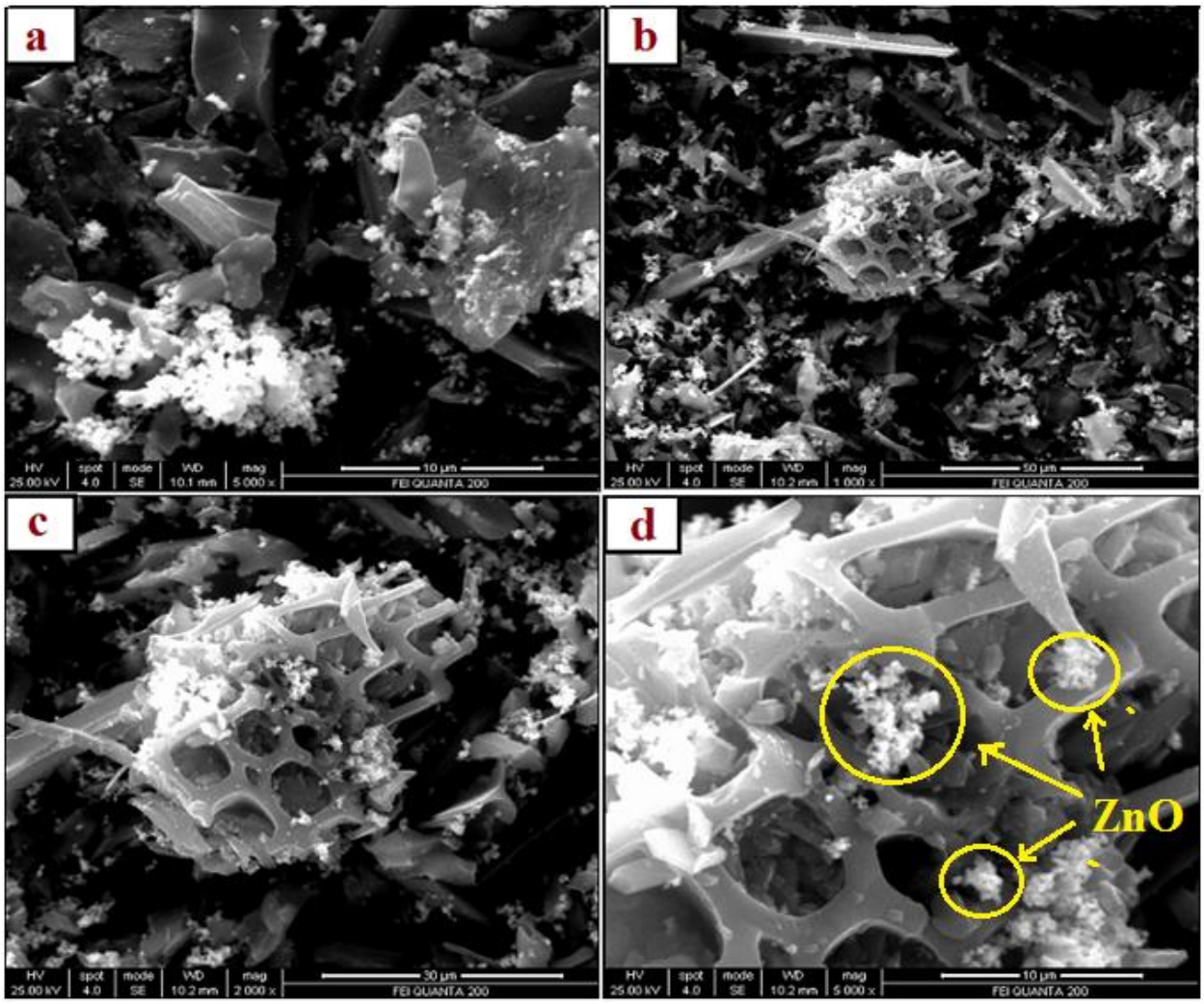

Figure 3 (a-d) SEM image of ZnO-AC nanoparticles

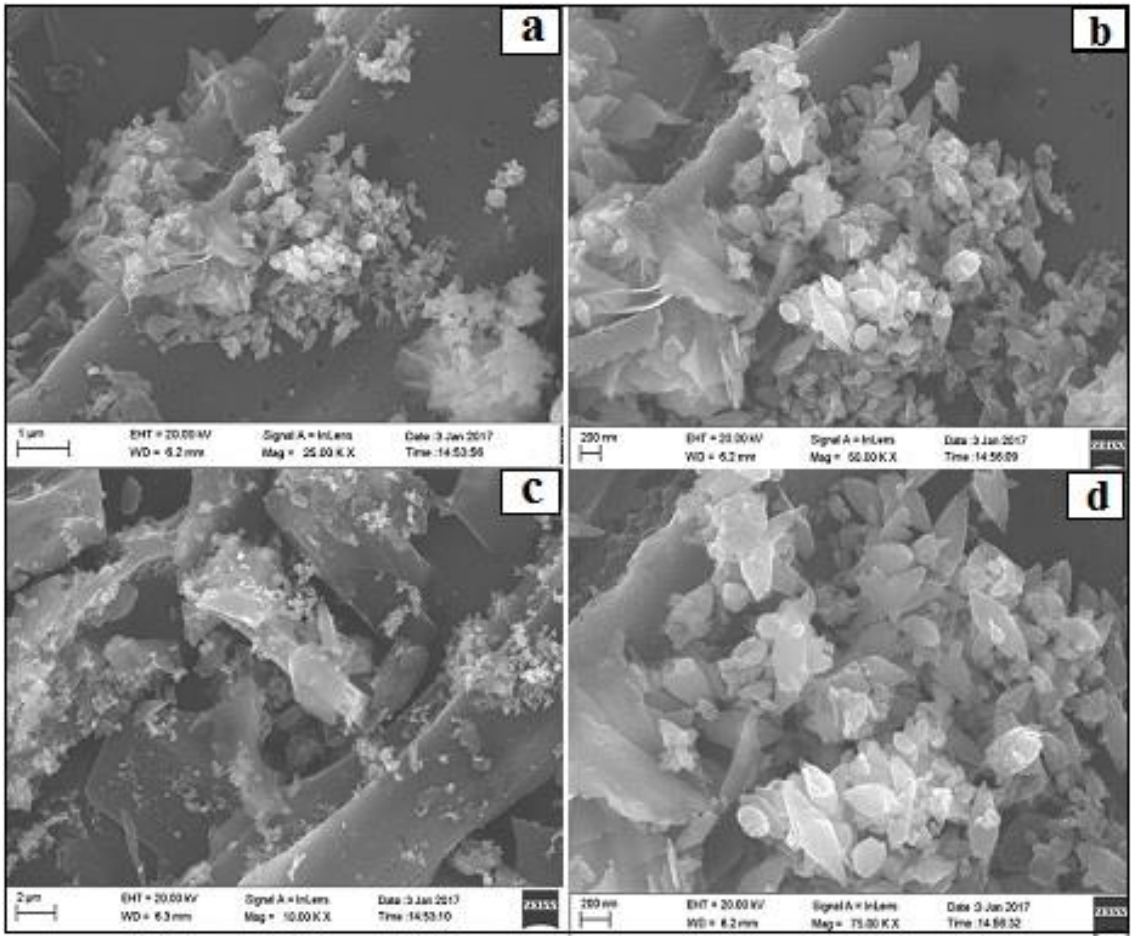

Figure 4 (a, b) SEM images of ZnO-AC nanoparticles after OG adsorption (c, d) SEM images of ZnO-AC nanoparticles after Rh- B adsorption.

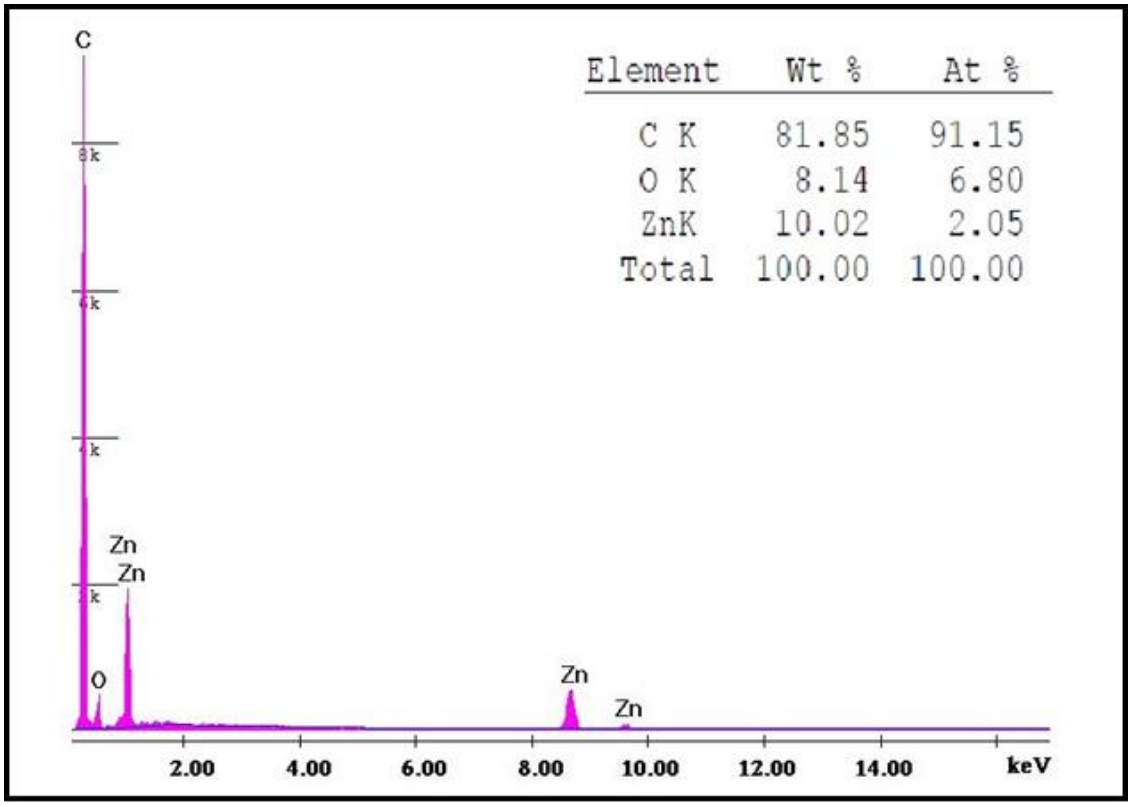

Figure 5 EDX of ZnO-AC nanoparticles

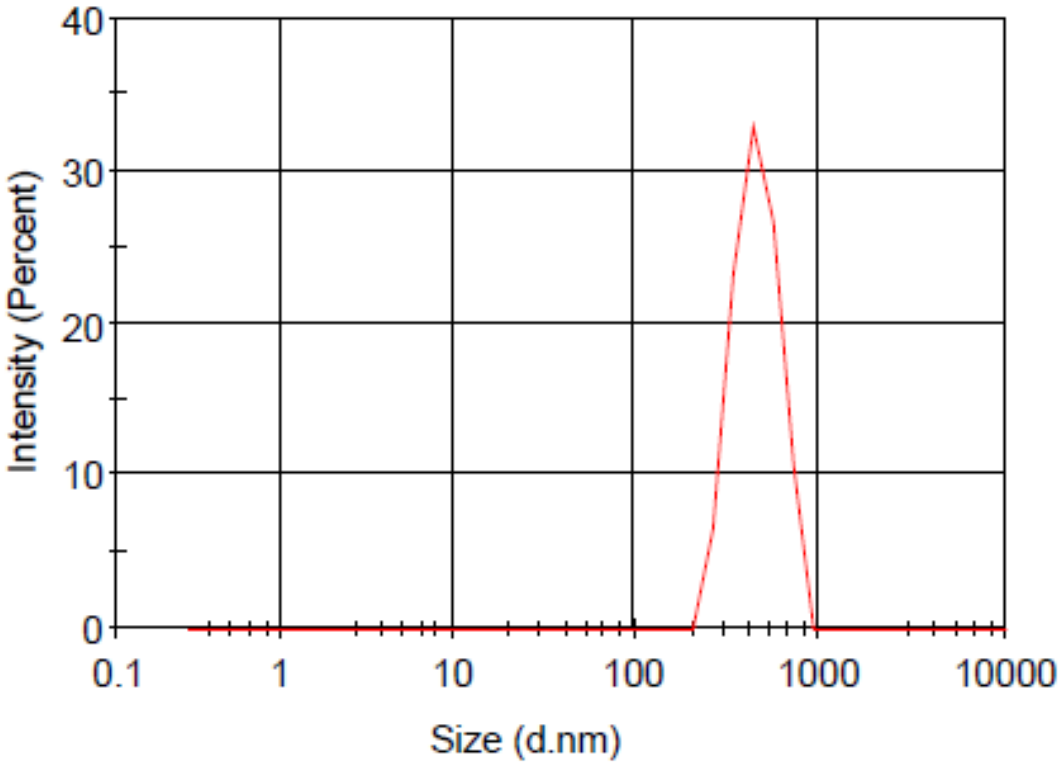

Figure 6 DLS of ZnO-AC nanoparticles

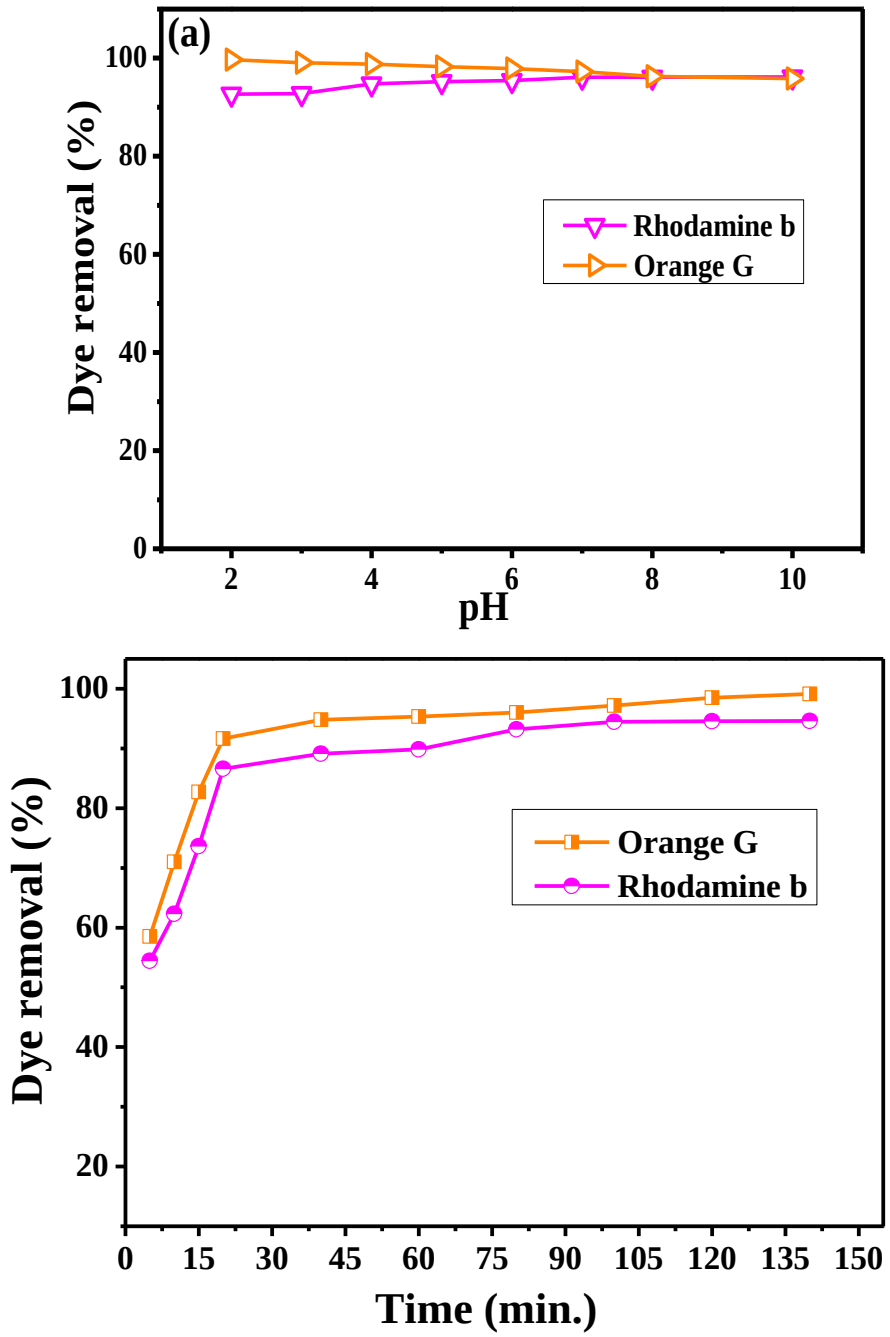

Figure 7 (a) Effect of pH on adsorption of Rh-B and OG dye on ZnO-AC nanoparticles (Experimental Conditions: dye conc.-50 mg/L, dose - 0.02g/50mL, temp. - 27˚C, contact time – 2 hours) (b) Effect of contact time adsorption of Rh-B and OG dye on ZnO-AC nanoparticles. (Experimental Conditions: pH – 7, dye conc.-50 mg/L, dose - 0.02g/50mL, temp. - 27˚C)

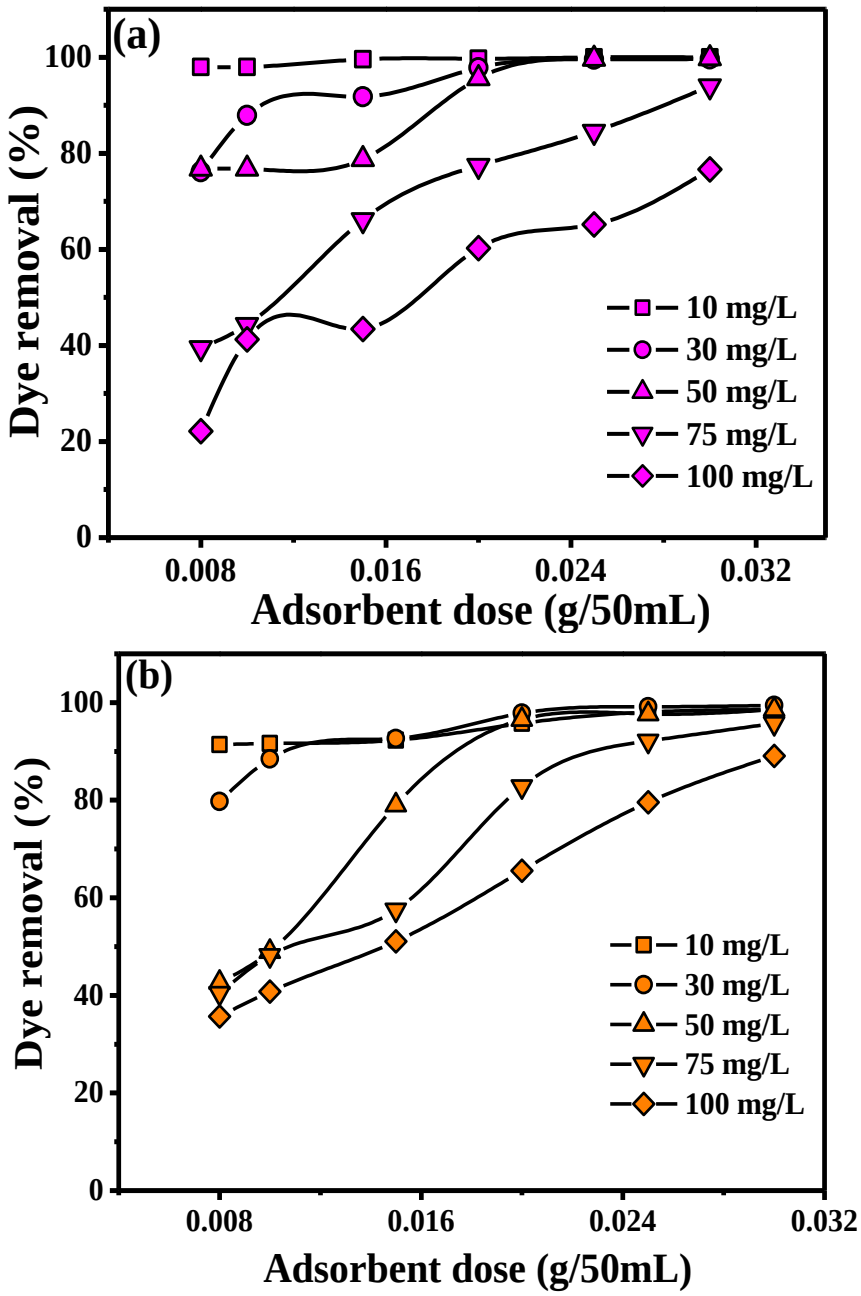

Figure 8 Adsorption of Rh-B and OG dye on ZnO-AC nanoparticles (a) effect of dye concentration with adsorbent dose for Rh-B (b) effect of dye concentration with adsorbent dose for OG. (Experimental Conditions: temp. -27˚C, contact time – 2 hours, pH – 7)

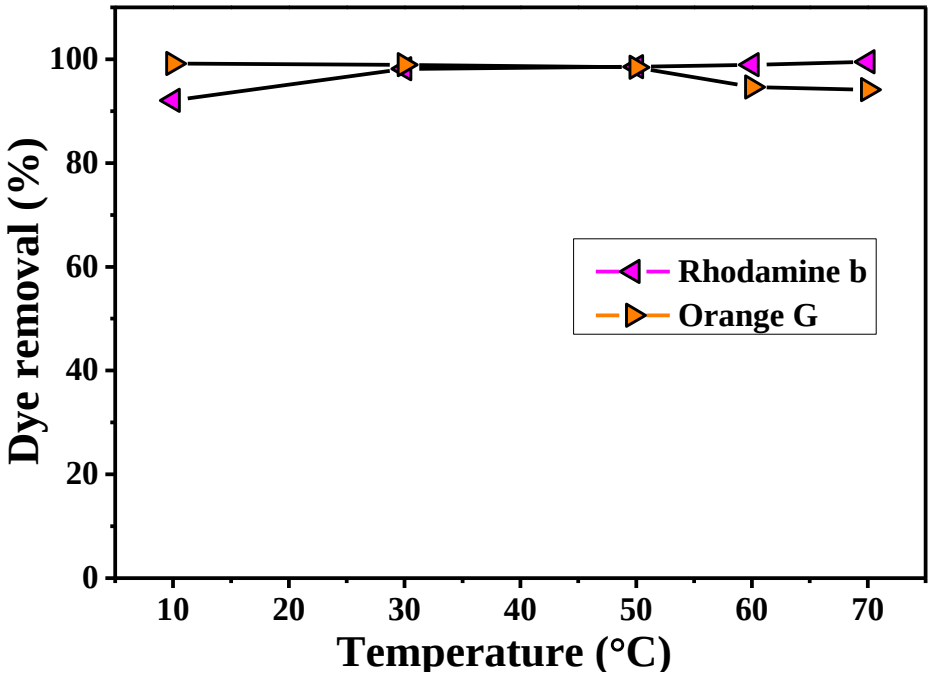

Figure 9 Effect of temperature for adsorption of Rh-B and OG dye on ZnO-AC nanoparticles. (Experimental Conditions: pH – 7, dye conc.-50 mg/L, dose - 0.02g/50mL)

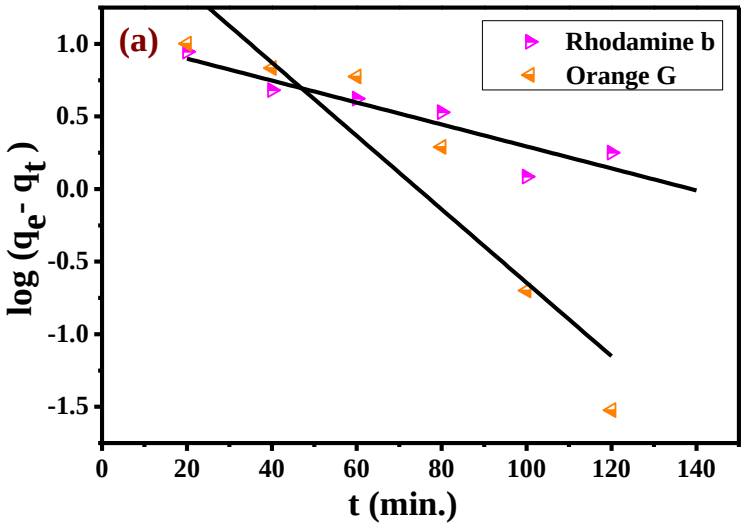

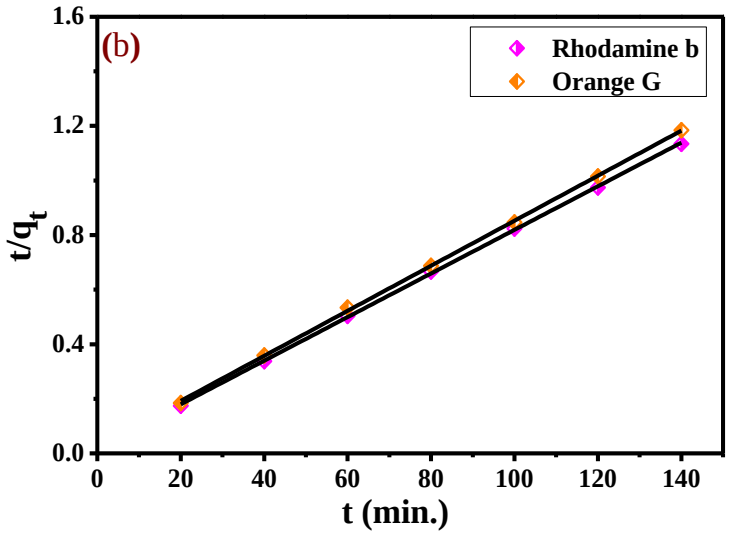

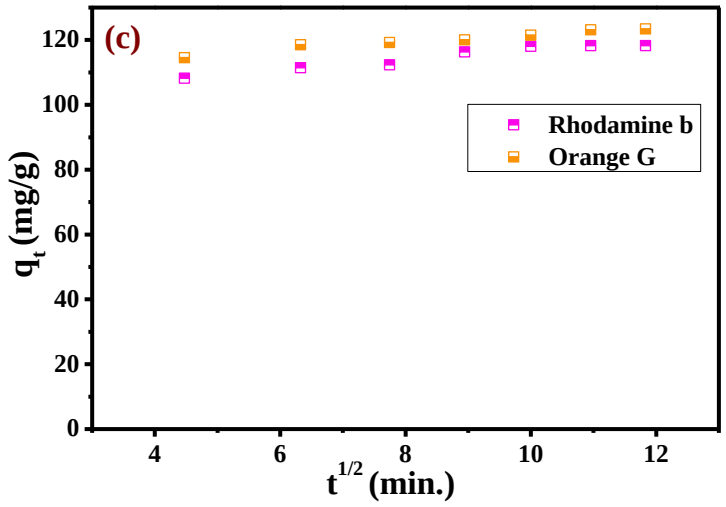

Figure 10 Kinetic plots for adsorption Rh-B and OG dye on ZnO-AC nanoparticles (a) pseudo-first order plot (b) pseudo-second order plot (c) intraparticle diffusion plot.

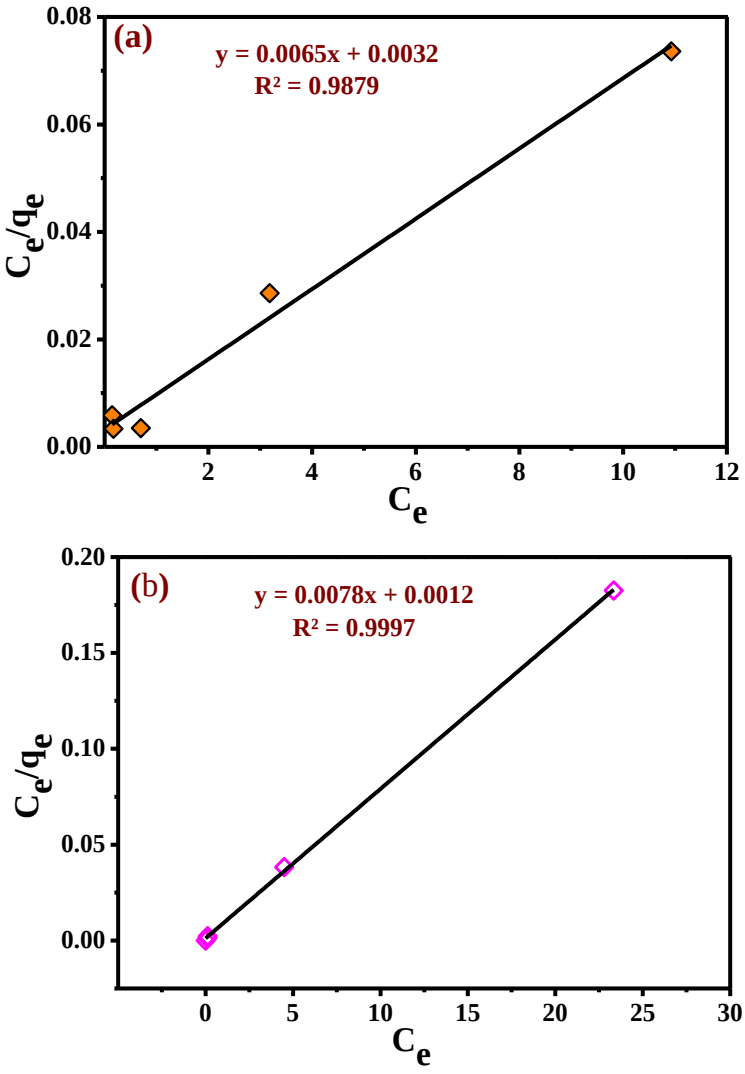

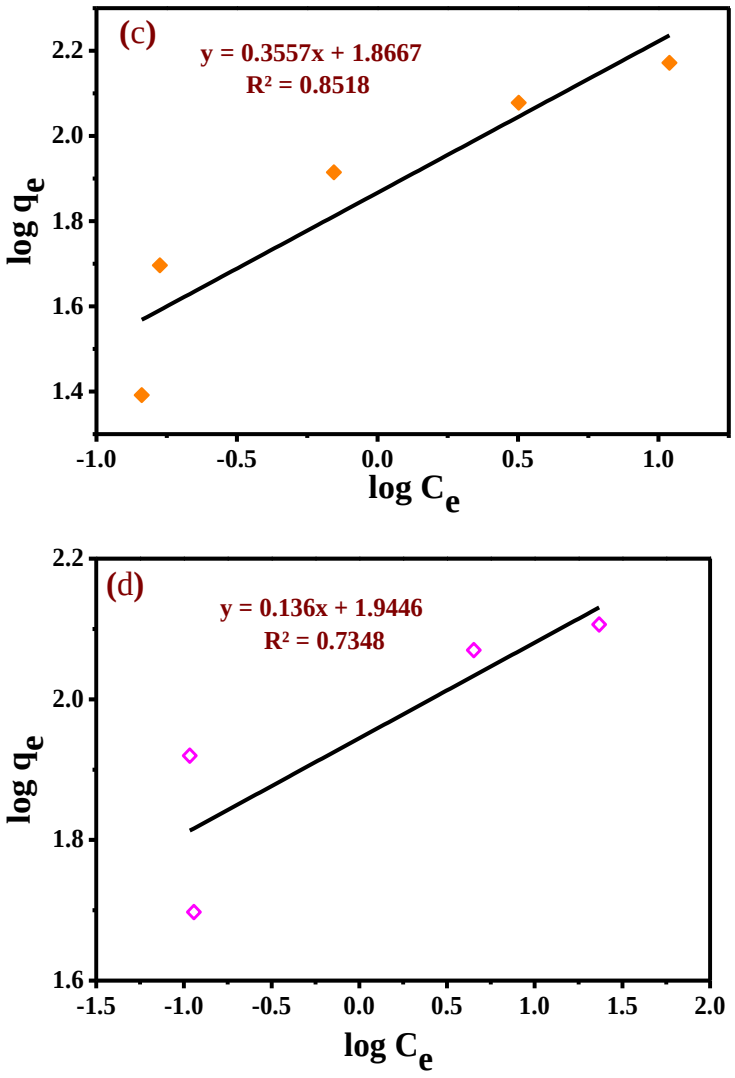

Figure 11 Adsorption isotherms plots for OG and Rh-B dye on ZnO-AC nanoparticles (a, b) Langmuir isotherm plot (c, d) Freundlich isotherm plot for OG and Rh-B dye respectively.

Table 1
Properties and structure of Rhodamine B and Orange G dyes

Dye	**Rhodamine B (Rh-B)**	**Orange G (OG)**
Molecular formula and structure	$C_{28}H_{31}ClN_2O_3$ 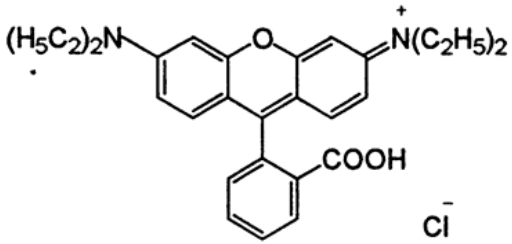	$C_{16}H_{10}N_2Na_2O_7S_2$ 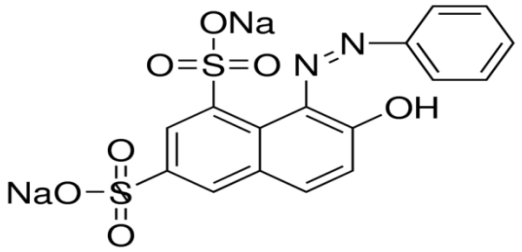
Molecular weight (g/mole)	479.01	452.37
Classification	Basic dye	Azo dye (N=N)
C.I. no	45170	16230
C.I. name	Basic Violet 10	Acid orange 10
Melting point (˚C)	210-211	---
Dye content (%)	≥ 95	90
λ_{max} (nm)	554	475

Table 2
Kinetic models parameters study for Rh-B and OG dye adsorption on ZnO-AC nanoparticles

Kinetic models	**Parameters**	**Values of parameters**	
		Rh-B	**OG**
Pseudo-first order	k_1 (min^{-1})	0.058	0.007
	q_e (cal)	76.37	11.34
	R^2	0.876	0.855
Pseudo-second order	k_2 (g/mg min)	0.0025	0.0032
	q_e (cal)	120.5	125.0
	R^2	0.999	0.999
Intraparticle diffusion	k_{id} (mg $g^{-1}min^{-1/2}$)	1.145	1.493
	C	110.2	101.8
	R^2	0.960	0.941
Experimental data	q_e (exp)	118.3	123.4

Table 3
Adsorptions isotherms model for Rh-B and OG dye adsorption interpreted by correlation coefficients and adsorption parameters.

Isotherms model	**Parameters**	**Parameters values**	
		Rh-B	**OG**
Langmuir	q_{max} (mg/g)	128.21	153.85
	b (L/mg)	6.50	2.03
	R^2	0.997	0.988
Freundlich	1/n	0.136	0.356
	K_f (mg/g)	88.02	73.57
	R^2	0.735	0.858

Table 4 Comparative study in adsorption capacity of various adsorbents for OG and Rh B dye

Adsorbent	**Dyes removed**	**$q_{max.}$ (mg/g)**	**Reference**
Parthenium Carbon	Rh-B	18.52	[14]
AC from industrial waste	Rh-B	16.12	[27]
Natural adsorbent Argemone Mexicana	Rh-B	6.4	[28]
ZnO nanorod loaded on activated carbon	Bromocresol Green Eosin Y	57.80 61.73	[12]
Fe_3O_4/HA	Rh-B	161.8	[29]
ZnO nanorod-loaded activated carbon	Malachite green Safranin O	59.17 55.25	[30]
Ag@AgBr/SBA-15	Rh-B	66.67	[31]
Magnetic bentonite material (Fe3O4/Al-B) Fe3O4	Rh-B	62.15 4.28	[32]
ZnS:Mn nanoparticles loaded on activated carbon	Direct Yellow 12 Reactive Orange 12	90.05 94.52	[33]
Bentonite material	OG	4	[34]
Prussian Blue nanoparticles supported over alumina	OG	44.4	[18]
ZnO-AC	OG	153.8	Present study
ZnO-AC	Rh-B	128.2	Present study

Table 5
Thermodynamic parameter description for Rh-B and OG dye adsorption over ZnO-AC nanoparticles.

Temperature (K)	Rhodamine-B (Rh-B) dye				Orange-G (OG) dye			
	ΔG^o (k J mol^{-1})	**$\ln(K_d)$**	**ΔS^o (J $mol^{-1}K^{-1}$)**	**ΔH^o (k J mol^{-1})**	**ΔG^o (k J mol^{-1})**	**$\ln(K_d)$**	**ΔS^o (J $mol^{-1}K^{-1}$)**	**ΔH^o (k J mol^{-1})**
283	-11.2088	4.764	57.192	28.043	-5.75996	2.448	-139.50	-33.310
303	-11.3846	4.519			-9.97121	3.958		
323	-11.0819	4.127			-11.3403	4.222		
333	-7.93253	2.865			-12.5118	4.519		
343	-7.94512	2.786			-14.9715	5.250		